

## Article

# Multi-Temporal Analysis of Past and Future Land-Cover Changes of the Third Pole

Munkhnasan Lamchin <sup>1,2,3</sup>, Woo-Kyun Lee <sup>4</sup>  and Sonam Wangyel Wang <sup>1,\*</sup><sup>1</sup> OJJeong Resilience Institute (OJERI), Korea University, Seongbuk-gu, Seoul 02841, Republic of Korea<sup>2</sup> Department of Environment and Forest Engineering, School of Engineering and Applied Sciences, National University of Mongolia, Ulaanbaatar City 14201, Mongolia<sup>3</sup> Institute for Sustainable Development, National University of Mongolia, Ulaanbaatar City 14201, Mongolia<sup>4</sup> Department of Environmental Science and Ecological Engineering, Korea University, Seongbuk-gu, Seoul 02841, Republic of Korea

\* Correspondence: wangsonam@korea.ac.kr

**Abstract:** In the past few decades, both natural and human influences have contributed to the unpredictable rates of land use and land-cover change (LUCC) in glacially devastated places. Monitoring and identifying the geographic and temporal land-cover changes and driving forces in this unique type of area may help to give the scientific basis needed to understand the effects of climate change and human activities on LUCC. The Third Pole is one such landscape that provides inevitable key ecosystem services to over 2 billion people in Asia. However, this important landscape is increasingly being threatened by the impacts of climate change. Policy and program responses to the Third Pole's mounting socioeconomic challenges are inadequate and lack scientific evidence. Using the land-change model (LCM) and historical data from 1992 onwards, our study attempted to (i) detect the spatial patterns of land use and land-cover changes in the Third Pole from 1992 to 2020; and (ii) project them into 2060. Our analysis shows that the land use and land-cover types in the Third pole are undergoing changes. About 0.07% of the snow and ice have melted in the last three decades, indicating global warming. This melt has resulted in increasing water bodies (0.08%), especially as glacial lakes. This has significantly increased the risk of glacial outburst floods. Other key alpine land-cover types that decreased are bare land (0.6%) and agricultural land (0.05%). These land types represent important habitats for wild flora and fauna, grazing land for livestock, and food for nomads, and their loss will directly degrade ecological services and the health and wellbeing of the nomads. Land cover of forest, shrubs, and scanty vegetation have all increased by 0.3%, 0.02%, and 0.77%, respectively, inducing socio-ecological changes in the Third pole mountains. Further predication analysis showed that snow and ice, along with bare land, will continue to recede whereas forest, grassland, water bodies, shrubland, sparse vegetation, and settlement will increase. These results indicate the increasing impact of global warming that will continue to change the Third Pole. These changes have serious implications for designing adaptation and mitigation interventions in the mountains. We recommend more detailed research to investigate the underlying factors that are changing the Third Pole to develop policy and programs to help humans, livestock, and biodiversity adapt to the changes in these remote and harsh mountains. This will also help to mitigate the effects on downstream communities.

**Keywords:** land-cover change; land-cover prediction; third pole; nomads; livestock; snow leopards; human wildlife conflicts



**Citation:** Lamchin, M.; Lee, W.-K.; Wang, S.W. Multi-Temporal Analysis of Past and Future Land-Cover Changes of the Third Pole. *Land* **2022**, *11*, 2227. <https://doi.org/10.3390/land11122227>

Academic Editor: Alexandru-Ionuț Petrișor

Received: 4 November 2022

Accepted: 4 December 2022

Published: 7 December 2022

**Publisher's Note:** MDPI stays neutral with regard to jurisdictional claims in published maps and institutional affiliations.



**Copyright:** © 2022 by the authors. Licensee MDPI, Basel, Switzerland. This article is an open access article distributed under the terms and conditions of the Creative Commons Attribution (CC BY) license (<https://creativecommons.org/licenses/by/4.0/>).

## 1. Introduction

The most fundamental and obvious landscape characteristic describing the influence of anthropogenic and natural disturbance on the surface of the Earth is changes in land use and land cover (LULC), which are significant in the studies of regional and global environmental changes [1]. Implementing and tracking Sustainable Development Goal (SDG) indicators,

such as changes in the extent of water-related ecosystems, land consumption rates, and the percentage of degraded land, are directly correlated with changes in land cover [2–4]. A dynamic LULC provides an inclusive understanding of the interactions and relationships that are essential for the management of sustainable land resources [5]. Understanding the LULC change drivers and dynamics is essential for creating sustainable strategies and making educated planning decisions. This was considered to produce an estimate of potential future scenarios in which the LULC change driving forces could be either direct or indirect for change through time and space [6]. High mountainous regions are most vulnerable to the impacts of global environmental and climate change due to their fragility. For instance, the Tibetan Plateau (TP), which is home to Earth's highest-altitude and the harshest and most sensitive climate, has experienced significant changes in the last several decades [7,8].

Outside of the Arctic and Antarctic, the Qinghai–Tibetan Plateau and the mountains that surround it are referred to as the Third Pole because of the amount of ice they hold [9]. More than 1.5 billion people receive fresh water, food, and other ecosystem services from the ten major rivers in Asia, which originate from these mountains [10,11]. The region's diverse topography and climate support a wide range of biological and social diversity. Unfortunately, the Third Pole region, along with Antarctica and the Arctic, is undergoing a considerably faster rate of air temperature increase than other places [10,12,13]. This warming is higher in the Third Pole mountains compared to the Arctic and Antarctic regions, resulting in the rapid melting of glaciers, snow, ice, and permafrost that unleashes disasters such as glacial lake outburst floods (GLOFs). In terms of socioeconomics, the Third Pole is predominantly agricultural, with many nomadic populations subsisting off of herding yaks, sheep, goats, etc. These nomads subsist entirely on the produce of their animals. Due to deteriorating pastures, dwindling water sources, and an increase in disasters that are made worse by global warming, raising livestock has become more and more challenging. The majority of the effects of the changing environment are being felt by nomads and their cattle. The environment surrounding the Third Pole is also a biodiversity hotspot that is home to threatened species such as the snow leopard and Tibetan wolf. Conflicts frequently arise between herders, livestock, and wildlife as a result of increased competition for grazing areas. In places where wolves and snow leopards have hurt livestock, people kill them in retaliation, putting biodiversity and ecological services at risk.

Although snow cover varies widely from year to year, it has diminished at lower elevations where snow has given way to rain [14]. The snow line, which is the elevation above which snow remains all year, has increasingly moved to higher elevations, leaving fewer areas covered with snow. This not only disrupts hydrological processes but also contracts habitats for snow biodiversity such as the snow leopards. In reaction to warming, snow-covered regions and snow volume will likely continue to decrease, and the snow line will continue to ascend to higher elevations [15]. Only a few studies have looked at variations in seasonal snow cover in Central Asia. They propose a reduction in the maximum snow depth and the duration of the snow cover [16]. In this study [17], authors examined snow cover in northern Central Asia using Advanced Very High-Resolution Radiometer (AVHRR) 1-km data for 1986–2008 and MODIS data for 2000–2009. The Central Asian republics, the Kazakh steppe, the Aral–Caspian desert, the Tarim, the Siberian Altai–Sayan, the Mongolian Altai, the Western Tian Shan, the Eastern Tian Shan, the Central Tian Shan, the Western Pamir, the Pamiro–Alai, the Central Pamir, and the Eastern Pamir were all included as high mountains. Asia would likely lose one-third of its glacier mass by the end of the century even if world average temperatures stabilized at 1.5 °C above pre-industrial levels, with the Himalaya losing half of its glacier mass [15,18]. Rapid melting of glaciers, snow, and ice disrupts social and ecological processes and unleashes disasters. High mountains of Asia experience a variety of disasters, including high-frequency landslides, floods, and coastal storms, as well as low-frequency earthquakes [19]. Additionally, there are increasing indications that human activity is having an adverse effect on the Third Pole's

ecosystem [20–22], which, together with projected changes in the future, could endanger the livelihoods of those who depend on the Third Pole’s resources and environment [23,24]. Continuity, which is required for continuing global challenges such as climate change, sustainable land management, and SDG implementation monitoring, is one of the key user requirements for GLC mapping. As a result, several mapping projects offer ongoing and operational land-cover solutions. For instance, the CCI-Land-cover product [25] provides annual GLC maps from 1992 to 2015 at a 300 m pixel scale. To increase classification accuracy, researchers have worked hard to develop cutting-edge methodologies and techniques, such as cellular automata, artificial neural networks, fuzzy logic, intelligent systems, and tree decisions [26]. The dynamics of natural and human systems are simulated, and their future evolution is predicted using object-based algorithms, such as CA [27]. It is effective at extracting realistic simulations of land use classes and other spatial structures despite its simplicity and can display remarkably rich behavior [27]. Previous works have extensively used this approach to identify LC classes [28–32]. Research has demonstrated the effectiveness of CA models in simulating land-cover patterns and other spatial structures in real-world settings. To anticipate LC changes utilizing descriptive characteristics such as elevation, slope, aspect, and distance from particular sites, the CA algorithm is an extension of the land change modeler (LCM) [33–36]. The land change modeler (LCM), although limited, successfully captured the dynamics of the simulated system and produced a simulation result that closely matched the reference map [37].

This research is probably the first attempt to employ a land change model (LCM) to assess and detect changes in the Third Pole, as well as to create LULC projections for the future. In particular, the study attempted to: (1) get multitemporal land-cover data; (2) look at the spatial and temporal changes of land cover in the Third Pole; (3) get and predict distribution patterns and look for general trends in land-cover changes; and (4) compare how land cover changed in each class over the study period.

## 2. Materials and Methods

### 2.1. Study Area

Based on information from the Global Land Ice Measurements from Space (GLIMS), high mountain range, and snow leopard range, we selected the study region. The idea of a Third Pole, where the temperature, biota, permafrost, and glaciers are such as those in the Arctic, has emerged as a result of the vast region of high altitudes in Central Asia, especially the Tibetan Plateau, which averages approximately 4500 m, and nearby mountain ranges (Figure 1). Permafrost, glaciers, ice, and snow make up the third-greatest reserve of fresh water in the Third Pole region. The Hindu Kush, Pamir, Tian Shan, and Kunlun ranges are all located in Central Asia. The Karakorum–Himalayan mountain range and Tibet are located in the southern region, which covers an area of more than 4.3 million km<sup>2</sup> and is shared by Afghanistan, Bangladesh, Bhutan, China, India, Myanmar, Nepal, and Pakistan [38]. The Himalayas, the Karakoram, the Tianshan, Kunlun, and Altai are the six greatest mountain ranges. It is home to 10 major river systems that flow through over 22 nations, including the Indus, Ganges, Brahmaputra, Irrawaddy, Salween, Mekong, Yangtze, Yellow, Tarim, and Amu Darya. It also features fourteen peaks that rise beyond 8000 m. This region has also been referred to as “the roof of the earth” because of its features, which include 36,800 glaciers and ice caps covering 49,870 km<sup>2</sup> and 1200 lakes (greater than 1 km<sup>2</sup>) covering an area of 47,000 km<sup>2</sup> [39,40]. The Greater Himalaya, which has peaks that average 6000 m and soar above 8500 m, the Lesser Himalaya, which is located in the middle, and the Lower Siwalik, which is located in the south, make up the 2500 km-long Himalaya. The Himalaya is 250–400 km wide overall. To the west of the Himalaya are the severely glacierized Karakorum ranges, which are 500 km long and 200 km wide. The southwest–northeast Kunlun mountains are located further west. The northwestern mountain ranges of Central Asia are the north–south Pamir of Tajikistan and the east–west Pamir–Alai of southern Uzbekistan–Kyrgyzstan. Together, they span 2000 km. With a height of 7400 m, the central Tian Shan is heavily covered in ice. The Alatau

ranges, which reach a height of about 5000 m, are part of the western Tian Shan. Whereas the northwest of the Pamir possesses alpine relief, the southwest is severely glacierized between 2500 and 5000–6000 m, including the 75 km-long Fedchenko Glacier. Peaks in the southeasterly Pamir range in height from 5000 to 5500 m.

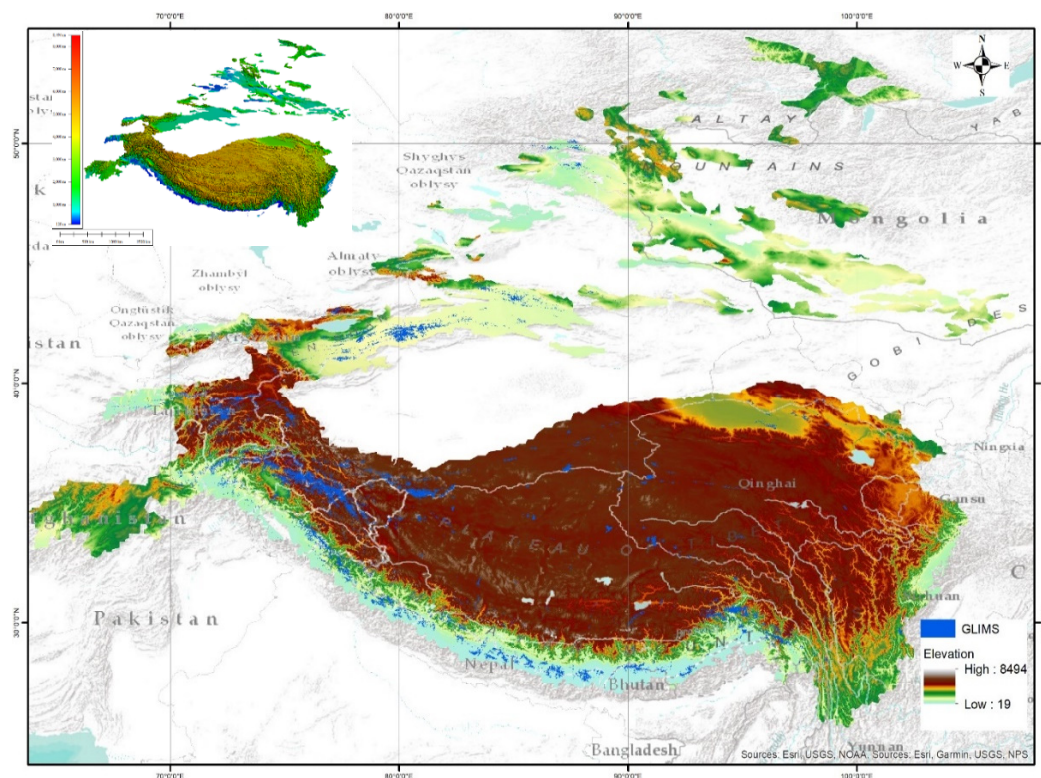


**Figure 1.** Study area of elevation map of the Third Pole and the snow leopard region of Asia.

## 2.2. Data and Preprocessing

### 2.2.1. Satellite Data Acquisition

We used the newly available annual ESA (European Space Agency) CCI (climate change initiative) land-cover maps to give continuous information about land-cover changes at a resolution of 300 m for the period between 1992 and 2020. This dataset's baseline was established by integrating the outcomes of machine learning and unsupervised techniques [41]. Using the United Nations Land-Cover Classification System (UN-LCCS), the ESA CCI represents the surface of planet Earth classified into 37 initial land-cover classes [42].

### 2.2.2. Preprocessing and Reclassification

This investigation included the following primary steps: (i) image reclassification and history LC map extraction; (ii) monitoring land-cover changes for historical maps; and (iii) LC change prediction by applying a land change modeler (LCM) that we showed in Figure 2.

In this study, we reclassified the ESA CCI LC classes based on the IPCC land categories as Table 1 [41] into ten distinct classes to detect and predict decadal change for the years 1992, 2000, 2010, and 2020, and the years 2030, 2040, 2050, and 2060, respectively. The ESA CCI LC product is comprised of 37 distinct land-cover classes; hence, every pixel in the land-cover image is assigned a class between 1 and 37. In order to reclassify the land-cover image in GRASS (Geographic Resources Analysis Support), a new mapset was built. Because the format of the data in GRASS is different from QGIS (Quantum GIS), the data were imported to the GRASS mapset with the `r.in.gdal` command (Import GDAL supported raster file into a binary raster map layer). The 37 subcategories were then reclassified into ten new classes

using the same GRASS command, *r.reclass*, as described in this manual [43] as Table 1. We integrated each class based on an increased understanding of how the LC class definitions are interpreted to calculate each LC class allocation. Regarding the accuracy assessment of reclassification, ESA-CCI-LC data already had accuracy assessment data; however, we performed an accuracy assessment for the reclassified map before in this study [44].

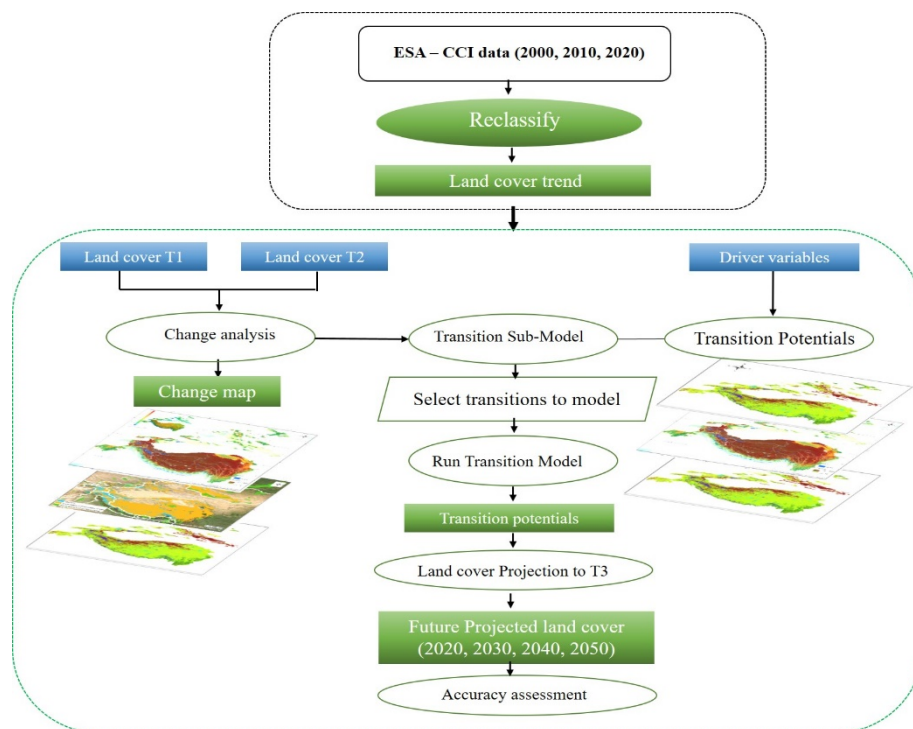


Figure 2. Flow Chart of Methodology.

Table 1. Classes of ESA and this study.

Category in Model	Code	LULC Class of ESA CCI
Cropland	10, 11, 12	Rainfed cropland
	20	Irrigated cropland
	30	Mosaic cropland (>50%)/natural vegetation (tree, shrub, herbaceous cover) (<50%)
	40	Mosaic <b>natural</b> vegetation (tree, shrub, herbaceous cover) (>50%)/cropland (<50%)
Forest	50	Tree cover, broadleaved, evergreen, closed to open (>15%)
	60, 61, 62	Tree cover, broadleaved, deciduous, closed to open (>15%)
	70, 71, 72	Tree cover, needle leaved, evergreen, closed to open (>15%)
	80, 81, 82	Tree cover, needle leaved, deciduous, closed to open (>15%)
	90	Tree cover, mixed leaf type (broadleaved and needle leaved)
	100	Mosaic tree and shrub (>50%)/herbaceous cover (<50%)
	160	Tree cover, flooded, fresh or brackish water
170	Tree cover, flooded, saline water	
Shrubland	110	Mosaic herbaceous cover (>50%)/tree and shrub (<50%)
	120, 121, 122	Shrubland
Grassland	130	Grassland
Sparse vegetation	140	Lichens and mosses
	150, 151, 152, 153	Sparse vegetation (tree, shrub, herbaceous cover)

Table 1. Cont.

Category in Model	Code	LULC Class of ESA CCI
Wetland	180	Shrub or herbaceous cover, flooded, fresh/saline/brackish water
Urban	190	Urban areas
Bare area	200, 201, 202	Bare areas
Water	210	Water bodies
Snow ice	220	Permanent snow, ice, and glacier

### 2.2.3. Land-Cover Change Model

A land change modeler (LCM) is an empirically driven, step-by-step approach [45] that performs change analysis, transition potential modeling, and change prediction based on the historical change from time 1 (2000) to time 2 (2010). Multi-Layer Perceptron Neural Network (MLP-NN) and Cellular Automata–Markov Chain models are combined in the prediction task (CA-MCM). Changes at the highest-ranking pixels in the transition potential maps have been verified by LCM, as demonstrated by [46]. Other studies [47,48] found that when explanatory factors generate disconnected patches with high transition potential, LCM tends to mimic new patches. In order to account for interactions between different variables, neural networks employ non-linear functions. To account for the fact that a single variable may have varying influences across the study area, the model might make use of machine learning techniques [49,50].

### 2.2.4. Change Analysis Module

Equations describing the CA-MC analysis module used to detect land-cover change between two years are provided below (Equation (2)) [51,52]:

$$S_{(t,t+1)=P_{ij}} \times S_{(t)} \quad (1)$$

where  $S_{(t)}$  is the system status at time of  $t$ ,  $S_{(t+1)}$  is the system status at time  $t + 1$ ; the matrix  $P_{ij}$  representing the probabilities of transition between states is determined by the formula [52,53]:

$$P_{ij} = \begin{pmatrix} P_{11} & P_{12} & \dots & P_{1n} \\ P_{21} & P_{22} & \dots & P_{2n} \\ \vdots & \vdots & \vdots & \vdots \\ P_{n1} & P_{n2} & \dots & P_{nn} \end{pmatrix}, (0 < P_{ij} < 1) \quad (2)$$

where  $P$  is the Markov probability matrix and  $P_{ij}$  is the transition probability from state  $I$  to  $j$  at the next time step. The probabilities of a low transition and a high transition are, roughly speaking, 0 and 1 [52,53]. Once the changes were classified as gains and losses to each land-cover category, transitions from one land-cover state to another were used to generalize the geographic altering pattern [54,55]. Categorical variables can be included in the analysis extremely well using the evidence likelihood transformation panel [56]. By calculating the relative frequency with which various land-cover types occur, evidence of likelihood was created.

### 2.2.5. MLP-NN Performance Evaluation

MLP-backpropagation NN's algorithm (BP) learning technique employs transition potential; forward and backward passes continue until the network acquires the characteristics of all classes [57]. Prior to performing any land-cover modification simulation, it is crucial to conduct a sensitivity analysis on the model, as the selection of appropriate variables affects the learning accuracy of the model [58]. Using the MLP classifier's image processing toolkit, parameters and model performance were tested. The model was trained procedurally using all explanatory factors and land cover; thereafter, the system repeatedly

executes skill tests to determine the relative effectiveness of explanatory variables while holding the inputs from specific variables constant [56]. Therefore, the skill gap informs us of the strength of that variable. To evaluate the skill  $S$  (Equation (3)), three distinct parameter sensitivity studies were conducted: forcing all independent variables except one to be constant; forcing a step-by-step constant forcing mechanism; and forcing all independent variables to be constant. The skill metric has a range of 1 to  $-1$ , with 1 indicating great forecasting,  $-1$  indicating worse than chance, and 0 indicating random chance [58].

$$s = \frac{(A - E(A))}{(1 - E(A))} \quad (3)$$

where  $A$  is measured accuracy, and  $E(A)$  is expected accuracy which is determined by using the number of transitions in the sub-model,  $T$  and the number of persistence classes,  $P$  as (Equation (4)):

$$E(A) = \frac{1}{(T + P)} \quad (4)$$

Using RMSE (Equation (5)), Ref. [59] evaluated the performance and prediction accuracy of the MLP-NN. RMSE is a measure of the variance between predicted and observed values. The lower the value, the more precise the forecast [59].

$$RMSE = \frac{\sqrt{\sum_{i=1}^N (u_i - u)^2}}{N} \quad (5)$$

where  $u_i$  is the modelled for sample  $i$ ,  $u_i$  is the observed data for sample  $i$  and  $N$  is the total number of samples.

#### 2.2.6. Transition Potential Modeling and Land-Cover-Change Prediction

Using RMSE (Equation (4)), Ref. [59] evaluated the performance and prediction accuracy of the MLP-NN. RMSE is a measure of the variance between predicted and observed values. The lower the value, the more precise the forecast [59]. The transition sub-model of the LCM was imported with skill-tested driving variables, and MLP-NN was then utilized to construct prospective transition maps utilizing the dependent variables (T1 and T2 images). At this time, the transition potential images adequately reflected the influence of the driver variables in determining if cell transformation was suitable for a certain land cover [51,58,60]. The driver elements were selected based on the literature review [61,62] and the author's experience with the subject area.

#### 2.2.7. Verification of Model Results

To verify the validity and acceptability of the MLP-CA-MC model in predicting future land cover [51,63], the validation method measured the current agreement and disagreement between the actual satellite-driven (T3) and simulated (T'3) LULC maps of 2020. In this investigation, both hard and soft predictions were used in two separate validations. The VALIDATE and ROC modules were utilized for this purpose. The T'3 soft prediction is used as a comparison map when calculating the area under the receiver operating characteristic curve (AUC) using ROC statistics [56]. AUC values range from 0 to 1, with 0 indicating an entirely inaccurate test and 1 indicating an entirely accurate test [57,64–67]. Using the T'3 hard prediction as a comparison map, the VALIDATE module calculates three types of kappa index statistics: kappa for grid cell level location (Klocation), kappa for no information (Kno), and kappa for stratum-level location (KlocationStratum), and kappa standard (Kstandard). Values of 80% or higher are generally associated with a significant and favorable AUC and kappa value [56–58]. In this study, the model is calibrated and validated using land-cover data from 2000 and 2010, after which a land-cover map for 2020 is simulated and validated using a reference land-cover map from 2020. Hits and Correct Rejection are the two components of agreement, whereas Misses, False Alarm, and Wrong Hits are the three components of disagreement.

### 3. Results and Discussion

#### 3.1. Modeling Verification

An essential need for research that tries to predict LULC changes is model validation [32,68]. The kappa statistic, which ranges from  $-1$  to  $+1$  [69], is a great example of frequently used techniques for determining a model's predictive power [70,71]. Other researchers [70,72] categorize kappa values as follows: 0 shows no agreement, 0.0–0.2 suggests slight agreement, 0.0–0.41 indicates poor agreement, 0.41–0.60 indicates moderate agreement, 0.60–0.80 indicates considerable agreement, and 0.81–1.0 indicates practically perfect agreement.

Based on the land-cover maps from 2000 and 2010, our study used the MLP-CA-MC model to: (i) simulate the soft and hard land-cover patterns in 2020, 2030, 2040, and 2050–2060 for validation purposes; and (ii) generate kappa statistics based on the comparison between the hard simulation and the 2020 reference map. The statistics show that Klocation, Kno, and Klocation Strata all have values of 82 percent, and the overall kappa value was 94.8 percent, which means that the simulated and observed land-cover maps agree perfectly.

There is a quantity disagreement when a cell amount that falls within the same category as  $T'3$  differs from  $T3$  [58]. Every time a cell in the same group as  $T'3$  differs from  $T3$ , there will be a location disagreement. The percentages of those who agree and disagree are shown in Figure 3. For MLP-CA-MC, the total components of disagreement were 15.9 percent, which is the sum of misses (8.7 percent) and false alarms (7.2 percent). The overall proportion of correct was 84.1 percent, which is the sum of hits (2.6 percent) and correct rejections (81.5 percent) (soft prediction). In the current study, a satisfactory after controlling for confounding variables, an AUC of 0.75 was found.

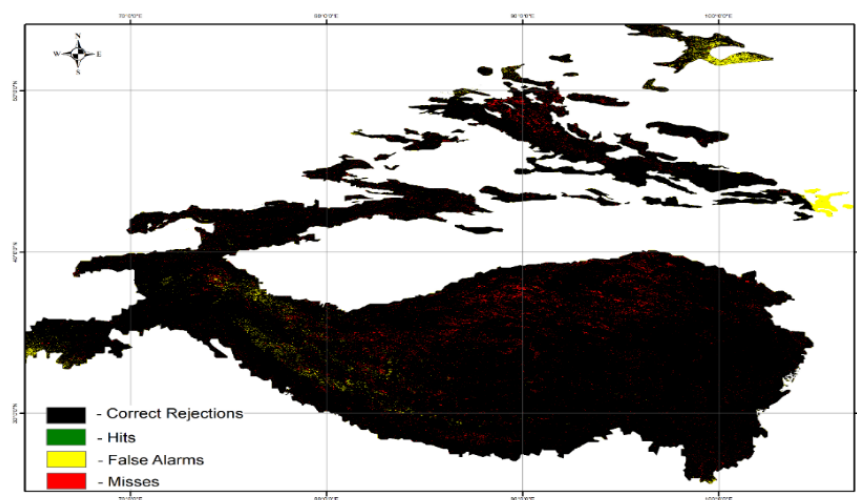


**Figure 3.** The quantity and allocation disagreement, showcasing the validation of the simulated map with the reference map.

#### 3.2. Land-Cover Monitoring and Changes of 1992–2020

Studies [40,54,73,74] have repeatedly demonstrated the Third Pole has been warming significantly in recent decades (annual rate of  $0.34$  °C/decade), with bigger trends than the Northern Hemisphere ( $0.29$ – $0.34$  °C/decade) and the global average ( $0.19$ – $0.34$  °C/decade). Since the latter half of the 20th century, this growth has been rapid, with warming rates quickly increasing from  $+0.16$  to  $+0.36$  °C/decade since the 1950s to  $+0.50$ – $+0.67$  °C/decade from the 1980s onward [75]. Further studies by [76] indicated that the Third Pole has warmed significantly between 1979 and 2020, with an annual rate of  $0.34$  °C/decade, which is higher than the rates for the northern hemisphere ( $0.29$  °C/decade) and the global average ( $0.19$  °C/decade) for the same period. Such amplifications could hasten changes in

the mountain ecosystem, cryosphere, hydrosphere, biodiversity, and nomads' way of life in the mountains of the Third pole and its surroundings [77–79].

We used land-cover data from 1992 to 2020, coinciding with exacerbated warming, to detect the observable impact of warming on land-use changes in the Third Pole. At the high altitudes, the Third Pole mountain landscape should ideally be dominated by cryosphere (snow, ice, permafrost), bareland, grassland, and sparse vegetation, with agriculture and forests in the lower pockets of the mountains. Spatiotemporal land-cover changes from 1992 to 2020 show overwhelming changes in the land-cover types in 2020 compared to 1992 (Table 2). Results indicate that the Third Pole was dominated by grassland, covering 56% of the land in 1992. This was followed by bare ground (20.1%), forest (8.63%), agriculture (6.22%), sparse vegetation (3.52%), snow and ice (2.98%), and water (1.26%). Except for high forest cover at that altitude, the statistics of land-cover types in 1992 were not far away from what is expected. Relative change from 1992 to 2020 showed a decrease in most of these dominant land types; for instance, bareland (−0.6%), grassland cover (−0.5%), snow and ice (−0.07), and agriculture (−0.05%). However, there was a significant increase in forested cover (0.3%), followed by spare vegetation (0.77%), and water (0.08%). All these changes are attributable to warming temperatures. Warmer climates provide more favorable conditions for trees, plants, and shrubs to thrive, especially in these very hard environments. The reduced coverage of snow and ice on grassland is attributable to global warming, and the melting of the latter may have increased water. Increasing water coverage in the mountains is dangerous and a sign of potential glacial lake outburst floods (GLOFs) in the future. Analyses at different time intervals between 1992 and 2020 allow us to investigate the direction and magnitude of how these changes have happened since 1992 (Table 2 and Figure 4); further, we showed the Third Pole's main transferred land-cover trends in the Figure 5.

Snow and ice decreased by 980 km<sup>2</sup> in 2000 compared to 1992. This decrease increased to 1154.0 km<sup>2</sup> between 2000 and 2010, followed by a slightly smaller decrease of 831.0 km<sup>2</sup> between 2010 and 2020. Overall, the Third Pole lost about 2965 km<sup>2</sup> of snow and ice in just three decades. Between 1992 and 2020, this melt increased the coverage of water bodies in the Third Pole by approximately 3335.8 km<sup>2</sup>. It can be concluded that human activities are involved in land-cover change and that the extreme sensitivity of glaciers to climate change often drives land-cover change processes in nonglacial locations. Furthermore, global climate change is a mutual feedback mechanism influenced by both human activity and land-cover change. More than in other parts of the world, places that have been impacted by glaciers feel the full force of the feedback loop between climate change, land-cover change, and human activity.

**Table 2.** Decadal Land-cover changes at the Third Pole from 1992 to 2020.

Land-Cover Type	Area Changes (km <sup>2</sup> )								Total Change	
	1992		2000		2010		2020		1992–2020	
	Area (km <sup>2</sup> )	Area (%)	Area (km <sup>2</sup> )	Area (%)	Area (km <sup>2</sup> )	Area (%)	Area (km <sup>2</sup> )	Area (%)	Area (km <sup>2</sup> )	Area (%)
Agriculture	255,490.4	6.22	258,701.1	6.30	255,607.7	6.22	253,381.0	6.17	−2109.4	−0.05
Forest	354,709.7	8.63	357,400.9	8.70	361,835.7	8.81	366,821.0	8.93	12,111.2	0.3
Grassland	23,17,869.0	56.4	2,307,435.6	56.2	2,315,319.1	56.4	2,297,093.1	55.9	−20,775.8	−0.5
Shrubland	26,815.9	0.65	27,115.3	0.66	27,263.4	0.66	27,505.4	0.67	689.5	0.02
Sparse vegetation	144,702.5	3.52	152,819.1	3.72	160,866.5	3.92	176,422.6	4.29	31,720.0	0.77
Wetland	8357.1	0.20	8522.5	0.21	8340.9	0.20	8351.0	0.20	−6.1	0.00
Settlement	464.8	0.01	532.7	0.01	986.3	0.02	1634.1	0.04	1169.3	0.03
Bareland	825,871.1	20.1	822,545.6	20.0	803,907.2	19.6	802,701.6	19.5	−23,169.5	−0.6
Water body	51,877.2	1.26	52,064.9	1.27	54,164.9	1.32	55,213.0	1.34	3335.8	0.08
Snow and ice	122,630.8	2.98	121,650.8	2.96	120,496.8	2.93	119,665.8	2.91	−2965.0	−0.07

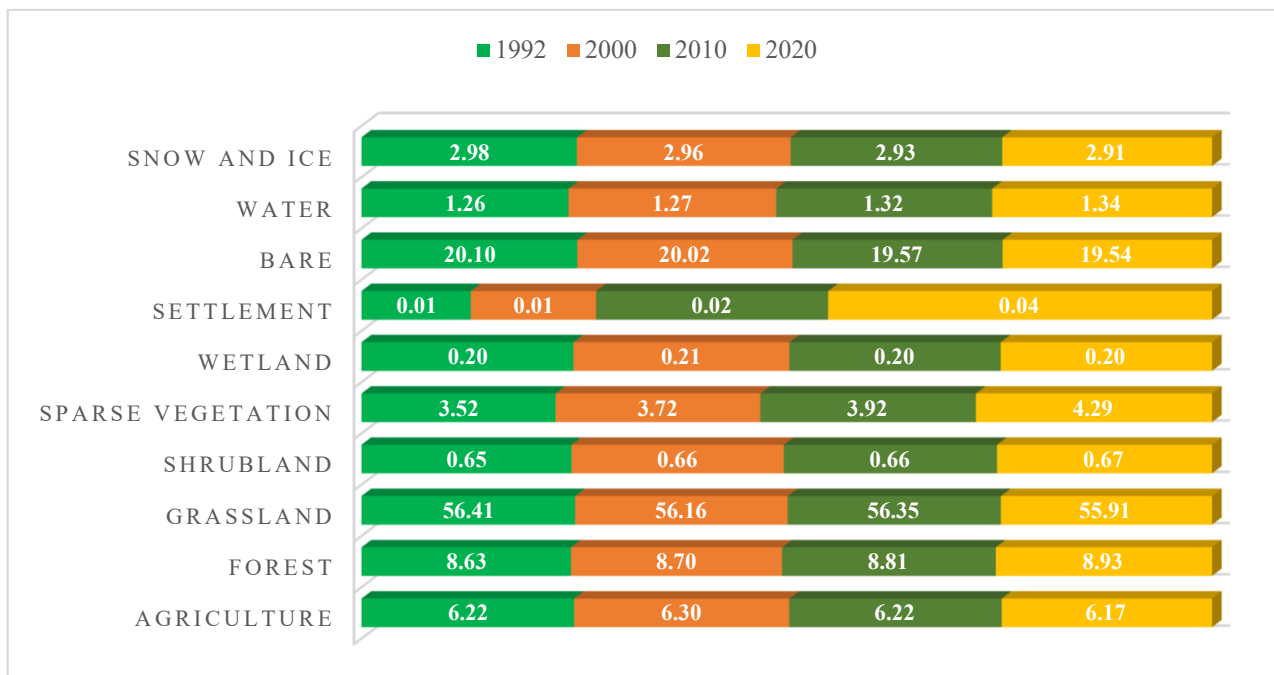


Figure 4. A graph shows the Third Pole’s decadal land-cover trends between 1992 and 2020 (Percent).

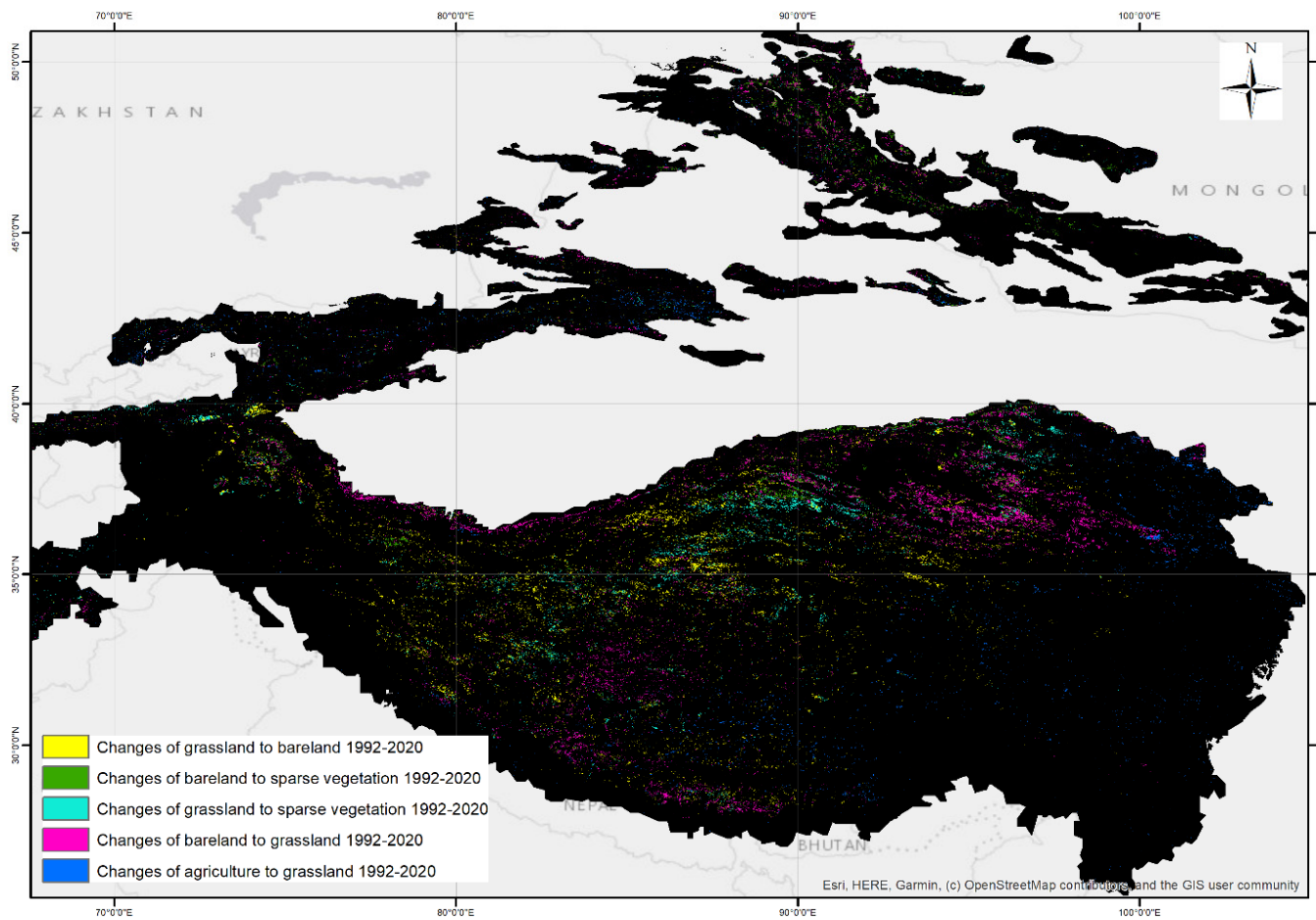


Figure 5. A map showing the Third Pole’s main transferred land-cover trends between 1992 and 2020.

This could be attributed to the initial melt probably being frozen into ice. A number of studies have also attributed an extraordinary shrinkage and negative mass balance of glaciers in several parts of the Third Pole [78,80–84] to global warming. Studies [76,85–87] have also found a general decrease in snow cover and depth, even though there are differences between regions and times of the year. In sync with the decreasing patterns of snow and ice, the water body increased the most between 2000 and 2010 (2100 km<sup>2</sup>), followed by 1048.1 km<sup>2</sup> between 2010 and 2020. This is an interesting finding as the amount of snow and ice melt was greater during the 1992–2000 period compared to the 2010–2020 period. Studies in Hindukush and the Tibetan plateau also indicated increasing water bodies primarily due to growing mass of glacial lakes and emergence of new glacial lakes [88].

Another important high-altitude resource that decreased significantly was grassland between 1992 and 2000, with a loss of 10,433.3 km<sup>2</sup> but grassland has continuous increasing from 2000 to 2010. However, due to the large decrease from 1992 to 2000, the total change from 1992 to 2020 showed a slight decrease in grassland cover (−0.5%). Specifically, grassland increased by 7883.4 km<sup>2</sup> between 2000 and 2010, but lost 18,225.9 km<sup>2</sup> between 2010 and 2020. Previous research [9,89] demonstrated that the Third Pole has experienced a threefold increase in the rate of global warming over the past 50 years. Meanwhile, natural grasslands in the region have been deteriorating since the 1980s, likely as a result of climate change, population increase, grazing pressure, and rodent damage [75,90–92]. In China, previous research [93] discovered that alpine-steppe vegetation increased significantly, particularly in low-coverage grasslands (30%), which grew by 10%. It is therefore likely that warming will raise the distribution and upper limit of alpine meadows [94–98]. The semi-humid southeast Tibetan Plateau had an increase in vegetation due to warming, whereas the dry and semi-arid northwest Tibetan Plateau saw a rise in vegetation due to increasing precipitation [93]. Grasslands are important, especially as habitats for wild flora and fauna, as well as grazing grounds for livestock. Livestock is the major source of food (meat, milk, cheese, and butter), energy (dung), transportation (draught energy), and for making clothing, tents, and containers (such as bags and even water storage) from hair and hide. The decrease in grassland was the most significant during the 1992–2000 period, with a loss of 10,433.4 km<sup>2</sup>. A similar decrease in grassland growth rate by 1.8 percent was also reported in China by other studies [99]. This decrease is accompanied by an overall increase in forest cover of 12,111.26 km<sup>2</sup> between 1992 and 2020, with an increasing rate of coverage during the period. Studies by [93] indicated that the forest area increased continuously after 1998 in the Third pole region. It is probable that the department's stringent implementation of conservation and management measures, as well as plantation activities, will have an impact. That is a good sign that the forest service's reforestation initiatives and management efforts have helped slow down the rate at which trees are being cut down.

This is a clear indication that warming temperatures are facilitating the trees to climb higher and perhaps take over grasslands. Barelands, including rocky outcrops, are a key characteristic of the high mountain landscapes and provide key ecological services to alpine flora and fauna.

Between 1992 and 2020, bareland in the Third Pole shrank by 23,169.56 km<sup>2</sup> with increasing intensity. This decrease was also matched with an increase in sparse vegetation and shrubland by 31,720.6 km<sup>2</sup> and 689.56 km<sup>2</sup>, respectively. Since 1992, areas with relatively little vegetation have grown the most, which is a clear sign that warming is helping plants grow.

Human settlements have also grown between 1992 and 2020 by 1169.3 km<sup>2</sup>. The settlements increased consistently between the periods 2000, 2010, and 2020 by 464.8, 532.7, 986.3, and 1635.1 km<sup>2</sup>, respectively. The trajectory indicates that the nomad population is increasing rapidly, resulting in more settlements. Population growth under limited resources and a changing climate can exert additional pressure on natural resources as well as reduce the adaptive capacity of social ecological systems, thereby making adaptation and

mitigation efforts difficult. Despite the growth in settlements, agricultural land coverage decreased, indicating a food security problem. Food in the mountains is scarce and limited by environmental conditions. Global warming can facilitate the growth of more crops and improve the food security situation. However, the declining agriculture in the Third Pole necessitates additional interventions. Wetland coverage bounced up and down with no consistent pattern. However, compared to the 1992 area, it has decreased by 8351 km<sup>2</sup> by 2020, indicating that wetlands are disappearing. Wetlands in high altitude areas provide vital ecological services, including ground water regulation, habitat for wetland fauna, and carbon sequestration, etc.

When discussing human-caused factors, population expansion must naturally come up first [100]. Population expansion should be identified as a key factor in LUCC because rising demands for both food and shelter encourage people to cultivate and develop more land. Human activities, especially those motivated primarily by economic goals, are another anthropogenic component that cannot be discounted. The improvement of productivity and production technologies have increased the impact of human actions on regional LUCC. Ground-use patterns have shifted as a result of human activities such as clearing of forests, overgrazing, reclaiming of barren land, and building [101].

### 3.3. Prediction of Decadal Changes in Land Cover at the Third Pole from 2020 to 2060

We predicted the LULC for 2030, 2040, 2050, and 2060 after the model had been successfully validated. Figure 6a–d and Table 3 show the results of the LULC prediction study for the Third Pole for the four decades (2020–2030, 2030–2040, 2040–2050, and 2050–2060). Between 2020 and 2060, bareland, agriculture, and snow and ice continued to decline, losing a total predicted area of 79,870.5 km (1.94%), 8295.5 (0.20%), and 3373.0 (0.08%), respectively. Despite a net loss of grassland during the 1992 to 2020 period, the prediction analysis showed a net gain of 42,161.2 km<sup>2</sup> of grassland in the Third Pole. Other land types have all increased, with forest land gaining the most (18,727.7 km) during the prediction period, followed by sparse vegetation (12,782.2 km), and water bodies (9054.1 km). Forest plantation efforts, especially in China, may have also added to this increase [102]. Settlements, which have also increased, mostly in lower valleys, have taken over agricultural lands, which could threaten food security.

According to the prediction analysis, grassland areas will continue to expand throughout the entire period, with the fastest growth occurring between 2020 and 2030, when they will increase by 30,153.3 km<sup>2</sup>, followed by 2030 to 2040, 2040 to 2050, and 2050 to 2060, when they will increase by 2458.4 km<sup>2</sup>, 6224.0 km<sup>2</sup>, and 3325.5 km<sup>2</sup>, respectively. This increase may impact the bareland flora and fauna but can benefit the ever-increasing livestock population in the Third Pole. Recent research indicates that climate change [103] and increasing precipitation [93] are significantly promoting plant growth on the Tibetan plateau of the Third Pole. During 2071–2100, relative to 1950–2005, both RCP4.5 and RCP8.5 forecast a 15.8-day and 34.1-day increase, respectively, in the average first leaf date of alpine vegetation [104]. This indicates that the grassland, wetland, settlement, bareground, and water body areas will continue to expand in the future. The period between 2020 and 2030 exhibited the rate of increase in wetland cover, whereas the increase in water surface area amounted to 2960 km<sup>2</sup>. In subsequent years, the region will lose its ice and snow cover (Table 3). Recent research using the CMIP6 model predicts that the annual mean snow water equivalent will continue to decrease at the Third Pole under all three scenarios. A previous study [105] suggested a significant decrease in snow cover area in the small watershed of the Indus basin by the end of the century under the warm–dry climate conditions of RCP8.5 scenarios. The simulation shows that the retreat of the Tian Shan glacier’s terminal will be gradual and dramatic up until 2040, and then rapid thereafter [106]. Under the warmer RegCM3 scenario, the Qiangtang No. 1 glacier on the Tibetan Plateau is projected to lose 11–18% of its area and 19–30% of its volume by 2050 [107]. According to models, two well-studied Himalayan glaciers in Nepal and India will disappear between 2050 and 2100 [108,109]. As glacier tongues retreat, over-deepening causes existing lakes to enlarge

and new lakes to form [110], resulting in a threat of glacial lake outburst floods that is projected to triple by the end of the century [88]. Enhanced precipitation and warming-induced glacier meltwater were linked to the simulated lake expansion and level rise [111].

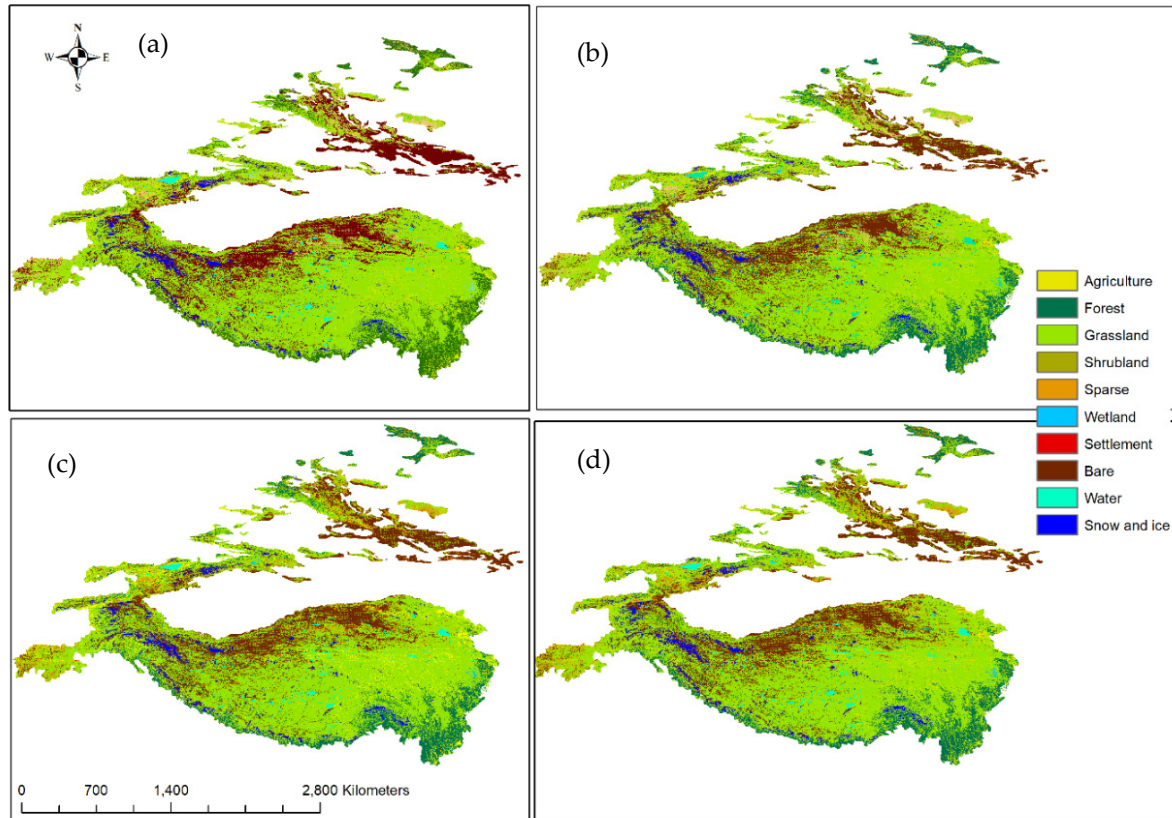


Figure 6. Predicted land-cover maps in (a) 2030; (b) 2040; (c) 2050; (d) 2060.

Table 3. Shows a decadal prediction of land-cover changes in the Third Pole from 2020 to 2060.

	Area Changes										Total Change	
	2020		2030		2040		2050		2060		2020–2060	
	Area (km <sup>2</sup> )	Area (%)										
Agriculture	253,381.0	6.17	250,762.2	6.10	248,665.2	6.05	246,790.2	6.01	245,085.5	5.96	−8295.5	−0.20
Forest	366,821.0	8.93	371,529.3	9.04	376,256.6	9.16	380,852.2	9.27	385,548.7	9.38	18,727.7	0.46
Grassland	2,297,093.1	55.9	2,327,246.4	56.6	2,329,704.9	56.7	2,335,928.8	56.9	2,339,254.3	56.9	42,161.2	1.03
Shrubland	27,505.4	0.67	27,763.7	0.68	28,172.8	0.69	28,336.3	0.69	28,734.1	0.70	1228.7	0.03
Sparse vegetation	176,422.6	4.29	171,759.1	4.18	177,988.9	4.33	183,874.2	4.48	189,204.8	4.60	12,782.2	0.31
Wetland	8351.0	0.20	10,790.4	0.26	13,397.2	0.33	13,997.5	0.34	14,475.8	0.35	6124.8	0.15
Settlement	1634.1	0.04	2003.4	0.05	2413.5	0.06	2653.9	0.06	3094.3	0.08	1460.2	0.04
Bareland	802,701.6	19.5	770,675.3	18.8	754,404.1	18.4	737,394.3	17.9	722,831.1	17.6	−79,870.5	−1.94
Water body	55,213.0	1.34	58,174.0	1.42	60,321.6	1.47	62,148.3	1.51	64,267.1	1.56	9054.1	0.22
Snow and ice	119,665.8	2.91	118,084.8	2.87	117,463.8	2.86	116,812.8	2.84	116,292.8	2.83	−3373.0	−0.08

We found that between 1992 and 2060, snow, ice and glacier cover, bareland, and agriculture decreased significantly due to climate change. Nevertheless, between 1992 and 2060, water bodies, settlements, and wetland and forest grew.

#### 4. Technical Significance and Limitations, Future Directions

The present investigation was conducted without major difficulties, but there were limitations. The first of these is that prediction analysis using the LCM model has not been evaluated at the regional scale, nor has prior research in the field been evaluated in the study area, whereas another is the adequacy of data collection and analysis. We determine the limits of this research area based on a number of primary factors. It is a

new boundary that includes the current international Third Pole boundary and the Tibet Plateau. Therefore, our boundary is larger than the boundaries of all other research studies pertaining to the Third Pole. Consequently, obtaining citations and comparing them with other studies is one of the difficulties. For a regional prediction and analysis of net change, only high-quality data should be selected, sectioned, and then combined. When figuring out the prediction and net change for a regional analysis, you must be very careful at every step because mistakes can be made at each step and add up over time.

## 5. Conclusions

The Third Pole landscape faces a serious challenge from global warming, which is significantly changing land use and land-cover types. Results indicate that from 1992 to 2060, the Third Pole experienced a decline in snow, ice, and glacier cover, bareland, and agriculture, as well as an increase in water bodies, settlements, wetland, and forest. Recognizing the driver variables of land-cover changes in the Third pole is important for enhancing the efficacy of conservation efforts to prevent further degradation of the region's unique ecosystem, which is why this study is so important. A proper management plan and strategy are required, as is the guarantee of their rigorous application. Continuous melting of the cryosphere, loss of bareland accompanied by increasing water bodies, forest cover and other vegetation types, and settlements indicate that the Third Pole is being impacted by global warming. Melting snow and ice (components of cryosphere) are seriously threatening access to water, food, and energy in the Third Pole mountains and river basins, significantly changing livelihood systems. LUC in the Third Pole was significantly influenced by human-caused climate change and other human-caused activities. The rate at which ice and snow cover melted was sped up by global warming, releasing a quantity of water resources further downstream. Further, the availability of water helped accelerate the pace of human development. The complicated coupling relationship between human activities and climate change is manifested in the Third Pole glacier-affected regions by LULC. High-altitude biodiversity is also threatened by habitat loss caused by a shrinking cryosphere, bareland, and expanding water bodies and forestland. In particular, significant loss of snow and bareland is a direct threat to the globally vulnerable snow leopard and other alpine flora and fauna. Changing biodiversity and ecosystem composition has socio-environmental consequences, including the degradation of key ecological services. Melting of the cryosphere directly leads to an increase in the number and volume of glacial lakes, thereby increasing the risk of glacial lake outburst floods that continue to inflict immense damage, including landslides, loss of agricultural land, infrastructure, properties, and human lives. This problem is further exacerbated by the increasing population, as indicated by the increasing settlements, who are directly dependent on natural resources. The increasing number of livestock to feed the increasing population degrades pastures and expedites alpine desertification. This competition also leads to conflicts between wildlife and herders when herds are killed by wildlife. The impact of global warming on the Third Pole in the absence of poor management policies and a lack of proper knowledge and early warning systems further worsens the situation. Our study shows that there is an urgent need to address adaptation and mitigation needs to secure water, food, energy security, and ecosystem integrity in the Third Pole, and this needs to be performed with urgency. It is a priority to conduct long-term scientific field research into more detailed land-use changes and disaster prediction in the Third Pole. We also suggest that a model specifically for detecting and predicting LULC in the Third Pole is needed.

**Author Contributions:** M.L. methodology, evaluation and results; writing original draft preparation; W.-K.L. Writing—review & editing, project administration; S.W.W. conceptualization of the study framework, development of the objectives, improvement of the original draft, review, language edits, and funding the research. All authors have read and agreed to the published version of the manuscript.

**Funding:** This research was funded by National Research Foundation of Korea’s Key Research Institute of Korea University, Republic of Korea.

**Acknowledgments:** The authors would like to thank the national research foundation of Korea for supporting the study.

**Conflicts of Interest:** The authors have declared that no competing interests exist.

## References

- Quintero-Gallego, M.E.; Quintero-Angel, M.; Vila-Ortega, J.J. Exploring land use/land cover change and drivers in Andean mountains in Colombia: A case in rural Quindío. *Sci. Total Environ.* **2018**, *634*, 1288–1299. [CrossRef] [PubMed]
- Romijn, E.; Herold, M.; Mora, B.; Briggs, S.; Seifert, F.M.; Paganini, M. Monitoring Progress towards: Sustainable Development Goals the Role of Land Monitoring. Wageningen, The Netherlands. 2016. Available online: [http://www.gofcgold.wur.nl/documents/newsletter/Sustainable\\_Development\\_Goals-infobrief.pdf](http://www.gofcgold.wur.nl/documents/newsletter/Sustainable_Development_Goals-infobrief.pdf) (accessed on 1 October 2022).
- UN-GGIM Global and Complementary (Non-Authoritative) Geospatial Data for SDGs: Role and Utilisation. 2019. Available online: [https://ggim.un.org/documents/Report\\_Global\\_and\\_Complementary\\_Geospatial\\_Data\\_for\\_SDGs.pdf](https://ggim.un.org/documents/Report_Global_and_Complementary_Geospatial_Data_for_SDGs.pdf) (accessed on 1 October 2022).
- Kavvada, A.; Ishida, C.; Juárez, J.; Ramage, S.; Merodio, P.; Friedl, L. EO4SDG. In *Earth Observation Applications and Global Policy Frameworks*; Kavvada, A., Cripe, D., Friedl, L., Eds.; Wiley: Hoboken, NJ, USA, 2022. [CrossRef]
- Mmbaga, N.E.; Munishi, L.K.; Treydte, A.C. How dynamics and drivers of land use/land cover change impact elephant conservation and agricultural livelihood development in Rombo, Tanzania. *J. Land Use Sci.* **2017**, *12*, 168–181. [CrossRef]
- Behera, M.D.; Borate, S.N.; Panda, S.N.; Behera, P.R.; Roy, P.S. Modelling and analyzing the watershed dynamics using Cellular Automata (CA)–Markov model—A geo-information based approach. *J. Earth Syst. Sci.* **2012**, *121*, 1011–1024. [CrossRef]
- Zhang, W.; Yi, Y.; Kimball, J.S.; Kim, Y.; Song, K. Climatic Controls on Spring Onset of the Tibetan Plateau Grasslands from 1982 to 2008. *Remote Sens.* **2015**, *7*, 16607–16622. [CrossRef]
- Wang, C.; Gao, Q.; Yu, M. Quantifying Trends of Land Change in Qinghai-Tibet Plateau during 2001–2015. *Remote Sens.* **2019**, *11*, 2435. [CrossRef]
- Qiu, J. China: The third pole. *Nature* **2008**, *454*, 393–396. [CrossRef]
- Yao, T.; Thompson, L.G.; Mosbrugger, V.; Zhang, F.; Ma, Y.; Luo, T.; Xu, B.; Yang, X.; Joswiak, D.R.; Wang, W.; et al. Third Pole Environment (TPE). *Environ. Dev.* **2012**, *3*, 52–64. [CrossRef]
- Molden, D.J.; Shrestha, A.B.; Immerzeel, W.W.; Maharjan, A.; Rasul, G.; Wester, P.; Wagle, N.; Pradhananga, S.; Nepal, S. The Great Glacier and Snow-Dependent Rivers of Asia and Climate Change: Heading for Troubled Waters. In *Water Security under Climate Change*; Springer: Berlin/Heidelberg, Germany, 2021; pp. 223–250. [CrossRef]
- EDW, M. Elevation-dependent warming in mountain regions of the world. *Nat. Clim. Chang.* **2015**, *5*, 424–430.
- Liu, X.; Cheng, Z.; Yan, L.; Yin, Z.-Y. Elevation dependency of recent and future minimum surface air temperature trends in the Tibetan Plateau and its surroundings. *Glob. Planet. Chang.* **2009**, *68*, 164–174. [CrossRef]
- Hock, R.; Rasul, G.; Adler, C.; Cáceres, B.; Gruber, S.; Hirabayashi, Y. High Mountain Areas. IPCC Special Report on the Ocean and Cryosphere in a Changing Climate. In *IPCC Special Report on the Ocean and Cryosphere in a Changing Climate*; IPCC: Geneva, Switzerland, 2019.
- Bolch, T.; Shea, J.M.; Liu, S.; Azam, F.M.; Gao, Y.; Gruber, S.; Immerzeel, W.W.; Kulkarni, A.; Li, H.; Tahir, A.A.; et al. Status and Change of the Cryosphere in the Extended Hindu Kush Himalaya Region. In *The Hindu Kush Himalaya Assessment*; Wester, P., Mishra, A., Mukherji, A., Shrestha, A., Eds.; Springer Science and Business Media LLC.: Cham, Switzerland, 2019; pp. 209–255.
- Unger-Shayesteh, K.; Vorogushyn, S.; Farinotti, D.; Gafurov, A.; Duethmann, D.; Mandychhev, A.; Merz, B. What do we know about past changes in the water cycle of Central Asian headwaters? A review. *Glob. Planet. Chang.* **2013**, *110*, 4–25. [CrossRef]
- Zhou, H.; Aizen, E.; Aizen, V. Seasonal snow cover regime and historical change in Central Asia from 1986 to 2008. *Glob. Planet. Chang.* **2017**, *148*, 192–216. [CrossRef]
- Wester, P.; Mishra, A.; Mukherji, A.; Shrestha, A.B. *The Hindu Kush Himalaya Assessment: Mountains, Climate Change, Sustainability and People*; Springer Nature: London, UK, 2019; p. 627.
- Vaidya, A.S.; Helander, J.D.M.; Peterson, F.C.; Elzinga, D.; Dejonghe, W.; Kaundal, A.; Park, S.-Y.; Xing, Z.; Mega, R.; Takeuchi, J.; et al. Dynamic control of plant water use using designed ABA receptor agonists. *Science* **2019**, *366*, eaaw8848. [CrossRef] [PubMed]
- IPCC. Intergovernmental Panel on Climate Change. Climate Change 2014: Synthesis Report. Available online: <http://www.ipcc.ch/> (accessed on 9 May 2016).
- Xiong, Q.; Xiao, Y.; Liang, P.; Li, L.; Zhang, L.; Li, T.; Pan, K.; Liu, C. Trends in climate change and human interventions indicate grassland productivity on the Qinghai–Tibetan Plateau from 1980 to 2015. *Ecol. Indic.* **2021**, *129*, 108010. [CrossRef]
- Feng, Y.; He, S.; Li, G. Interaction between urbanization and the eco-environment in the Pan-Third Pole region. *Sci. Total Environ.* **2021**, *789*, 148011. [CrossRef]
- Gioli, G.; Thapa, G.; Khan, F.; Dasgupta, P.; Nathan, D.; Chhetri, N.; Adhikari, L.; Mohanty, S.K.; Aurino, E.; Scott, L.M. Understanding and Tackling Poverty and Vulnerability in Mountain Livelihoods in the Hindu Kush Himalaya. *Hindu Kush Himalaya Assess.* **2019**, 421–455. [CrossRef]

24. Yang, M.; Dong, S.; Dong, Q.; Xu, Y.; Zhi, Y.; Liu, W.; Zhao, X. Trade-offs in ecological, productivity and livelihood dimensions inform sustainable grassland management: Case study from the Qinghai-Tibetan Plateau. *Agric. Ecosyst. Environ.* **2021**, *313*, 107377. [CrossRef]
25. CCI Land Cover Release of a 1992–2015 Time Series of Annual Global Land Cover Maps at 300 m. 2017. Available online: [https://www.esa-landcover-cci.org/index.php?q=webfm\\_send/88](https://www.esa-landcover-cci.org/index.php?q=webfm_send/88) (accessed on 1 October 2022).
26. Moran, E.; Brondizio, E.; Mausel, P.; Lu, D. Change Detection Techniques. *Int. J. Remote Sens.* **2004**, *25*, 2365–2407.
27. Marceau, D.J.; Wang, F.; Wijesekara, N. Investigating Land-Use Dynamics at the Periphery of a Fast-Growing City with Cellular Automata at Two Spatial Scales. In *Modeling of Land-Use and Ecological Dynamics 2013*; Springer: Berlin/Heidelberg, Germany, 2013; pp. 51–79. [CrossRef]
28. Etemadi, H.; Smoak, J.M.; Karami, J. Land use change assessment in coastal mangrove forests of Iran utilizing satellite imagery and CA–Markov algorithms to monitor and predict future change. *Environ. Earth Sci.* **2018**, *77*, 208. [CrossRef]
29. Feng, K.; Siu, Y.L.; Guan, D.; Hubacek, K. Assessing regional virtual water flows and water footprints in the Yellow River Basin, China: A consumption based approach. *Appl. Geogr.* **2012**, *32*, 691–701. [CrossRef]
30. Ozturk, D. Urban Growth Simulation of Atakum (Samsun, Turkey) Using Cellular Automata-Markov Chain and Multi-Layer Perceptron-Markov Chain Models. *Remote Sens.* **2015**, *7*, 5918–5950. [CrossRef]
31. Kalkhajeh, R.G.; Jamali, A.A. Analysis and Predicting the Trend of Land Use/Cover Changes Using Neural Network and Systematic Points Statistical Analysis (SPSA). *J. Indian Soc. Remote Sens.* **2019**, *47*, 1471–1485. [CrossRef]
32. Islam, K.; Rahman, F.; Jashimuddin, M. Modeling land use change using Cellular Automata and Artificial Neural Network: The case of Chunati Wildlife Sanctuary, Bangladesh. *Ecol. Indic.* **2018**, *88*, 439–453. [CrossRef]
33. Peraza-Castro, M.; Ruiz-Romera, E.; Meaurio, M.; Sauvage, S.; Sánchez-Pérez, J. Modelling the impact of climate and land cover change on hydrology and water quality in a forest watershed in the Basque Country (Northern Spain). *Ecol. Eng.* **2018**, *122*, 315–326. [CrossRef]
34. Gu, Q.; Hu, H.; Ma, L.; Sheng, L.; Yang, S.; Zhang, X.; Zhang, M.; Zheng, K.; Chen, L. Characterizing the spatial variations of the relationship between land use and surface water quality using self-organizing map approach. *Ecol. Indic.* **2019**, *102*, 633–643. [CrossRef]
35. Sangermano, F.; Toledano, J.; Eastman, J.R. Land cover change in the Bolivian Amazon and its implications for REDD+ and endemic biodiversity. *Lands. Ecol.* **2012**, *27*, 571–584. [CrossRef]
36. Gupta, R.; Sharma, L.K. Efficacy of Spatial Land Change Modeler as a forecasting indicator for anthropogenic change dynamics over five decades: A case study of Shoolpaneshwar Wildlife Sanctuary, Gujarat, India. *Ecol. Indic.* **2020**, *112*, 106171. [CrossRef]
37. García-Álvarez, D.; Olmedo, M.T.C.; Van Delden, H.; Mas, J.-F.; Paegelow, M. Comparing the structural uncertainty and uncertainty management in four common Land Use Cover Change (LUCC) model software packages. *Environ. Model. Softw.* **2022**, *153*, 105411. [CrossRef]
38. Barry, R.G.; Hall-McKim, E.A. *Polar Environments and Global Change*; Cambridge University Press: Cambridge, UK, 2018. [CrossRef]
39. Yao, T.; Wang, Y.; Liu, S.; Pu, J.; Shen, Y.; Lu, A. Recent glacial retreat in High Asia in China and its impact on water resource in Northwest China. *Sci. China Ser. D Earth Sci.* **2004**, *47*, 1065–1075. [CrossRef]
40. Deliang, C.; Baiqing, X.; Tandong, Y.; ZhengTang, G.U.; Peng, C.U.; FaHu, C.H.; Zhang, R.; Zhang, X.; Zhang, Y.; Jie, F.A. Assessment of Past, Present and Future Environmental Changes on the Tibetan Plateau. *Chin. Sci. Bull.* **2015**, *60*, 3025–3035.
41. ESA (European Space Agency). Land Cover, CCI. Product User Guide Version 2.0. 2017. Available online: [http://maps.elie.ucl.ac.be/CCI/viewer/download/ESACCI-LC-Ph2-PUGv2\\_2.0.pdf](http://maps.elie.ucl.ac.be/CCI/viewer/download/ESACCI-LC-Ph2-PUGv2_2.0.pdf) (accessed on 10 November 2017).
42. Di Gregorio, A. *Land Cover Classification System: Classification Concepts and User Manual: LCCS*; Food and Agriculture Organization: Rome, Italy, 2005; Volume 2.
43. ESCAP; United Nation. *Producing Land Cover Change Maps and Statistics: Guide on Advanced Use of QGIS and RStudio*; ESCAP: Bangkok, Thailand, 2021.
44. Lamchin, M.; Bilintoh, T.M.; Lee, W.-K.; Ochir, A.; Lim, C.-H. Exploring spatio-temporal change in global land cover using categorical intensity analysis. *Front. For. Glob. Chang.* **2022**, *5*, 994713. [CrossRef]
45. Eastman, J.R. *TerrSet Manual: Geospatial Monitoring and Modeling System*; Clark Labs Clark University: Worcester, MA, USA, 2016; p. 470.
46. Olmedo, M.T.C.; Paegelow, M.; Mas, J.F. Interest in intermediate soft-classified maps in land change model validation: Suitability versus transition potential. *Int. J. Geogr. Inf. Sci.* **2013**, *27*, 2343–2361. [CrossRef]
47. Mas, J.F.; Kolb, M.; Houet, T.; Paegelow, M.; Camacho Olmedo, M.T. Eclairer le choix des outils de simulation des changements des modes d’occupation et d’usages des sols. Une approche comparative. *Rev. Int. Geomat.* **2011**, *3*, 405–430. [CrossRef]
48. Mas, J.-F.; Kolb, M.; Paegelow, M.; Olmedo, M.T.C.; Houet, T. Inductive pattern-based land use/cover change models: A comparison of four software packages. *Environ. Model. Softw.* **2014**, *51*, 94–111. [CrossRef]
49. Mas, J.F.; Puig, H.; Palacio, J.L.; Sosa-Lopez, A. Modelling deforestation using GIS and artificial neural networks. *Environ. Model. Softw.* **2004**, *19*, 461–471. [CrossRef]
50. Olmedo MT, C.; Pontius Jr, R.G.; Paegelow, M.; Mas, J.F. Comparison of simulation models in terms of quantity and allocation of land change. *Environ. Model. Softw.* **2015**, *69*, 214–221. [CrossRef]

51. Kafy, A.-A.; Naim, N.H.; Subramanyam, G.; Faisal, A.-A.; Ahmed, N.U.; Al Rakib, A.; Kona, M.A.; Sattar, G.S. Cellular Automata approach in dynamic modelling of land cover changes using RapidEye images in Dhaka, Bangladesh. *Environ. Chall.* **2021**, *4*, 100084. [[CrossRef](#)]
52. Wang, S.W.; Munkhnasan, L.; Lee, W.K. Land use and land cover change detection and prediction in Bhutan's high-altitude city of Thimphu, using cellular automata and Markov chain. *Environ. Chall.* **2021**, *2*, 100017. [[CrossRef](#)]
53. Kumar, S.; Radhakrishnan, N.; Mathew, S. Land use change modelling using a Markov model and remote sensing. *Geomat. Nat. Hazards Risk* **2013**, *5*, 145–156. [[CrossRef](#)]
54. Kang, S.; Xu, Y.; You, Q.; Flügel, W.-A.; Pepin, N.; Yao, T. Review of climate and cryospheric change in the Tibetan Plateau. *Environ. Res. Lett.* **2010**, *5*, 015101. [[CrossRef](#)]
55. Leta, M.K.; Demissie, T.A.; Tränckner, J. Hydrological Responses of Watershed to Historical and Future Land Use Land Cover Change Dynamics of Nashe Watershed, Ethiopia. *Water* **2021**, *13*, 2372. [[CrossRef](#)]
56. Eastman, J.R. *TerrSet Geospatial Monitoring and Modeling System*; Clark University: Worcester, MA, USA, 2016; pp. 345–389.
57. Mandrekar, J.N. Receiver Operating Characteristic Curve in Diagnostic Test Assessment. *J. Thorac. Oncol.* **2010**, *5*, 1315–1316. [[CrossRef](#)] [[PubMed](#)]
58. Gharaibeh, A.; Shaamala, A.; Obeidat, R.; Al-Kofahi, S. Improving land-use change modeling by integrating ANN with Cellular Automata-Markov Chain model. *Heliyon* **2020**, *6*, e05092. [[CrossRef](#)] [[PubMed](#)]
59. Elçiçek, H.; Akdoğan, E.; Karagöz, S. The use of artificial neural network for prediction of dissolution kinetics. *Sci. World J.* **2014**, *2014*, 194874. [[CrossRef](#)]
60. Balogun, I.A.; Ishola, K.A. Projection of Future Changes in Landuse/Landcover Using Cellular Automata/Markov Model over Akure City, Nigeria. *J. Remote Sens. Technol.* **2017**, *5*, 22–31. [[CrossRef](#)]
61. Camara, M.; Jamil, N.; Abdullah, A.; Hashim, R. Integrating cellular automata Markov model to simulate future land use change of a tropical basin. *Glob. J. Environ. Sci. Manag.* **2020**, *6*, 403–414. [[CrossRef](#)]
62. Razaai, N.H.; Abdullah, S.A.; Reza, M.I.H. Identifying factors and predicting the future land-use change of protected area in the agricultural landscape of Malaysian peninsula for conservation planning. *Remote Sens. Appl. Soc. Environ.* **2020**, *18*. [[CrossRef](#)]
63. Dey, N.N.; Al Rakib, A.; Kafy, A.A.; Raikwar, V. Geospatial modelling of changes in land use/land cover dynamics using Multi-layer perception Markov chain model in Rajshahi City, Bangladesh. *Environ. Chall.* **2021**, *4*, 100148. [[CrossRef](#)]
64. Pontius, R.G., Jr.; Millones, M. Death to Kappa: Birth of quantity disagreement and allocation disagreement for accuracy assessment. *Int. J. Remote Sens.* **2011**, *32*, 4407–4429. [[CrossRef](#)]
65. Pontius, R.G., Jr.; Peethambaram, S.; Castella, J.C. Comparison of three maps at multiple resolutions: A case study of land change simulation in Cho Don District, Vietnam. *Ann. Assoc. Am. Geogr.* **2011**, *101*, 45–62. [[CrossRef](#)]
66. Varma, P.K. Application of EuroSCORE II and STS score for risk assessment in Indian patients—Are they useful? *Indian J. Thorac. Cardiovasc. Surg.* **2021**, *37*, 716–717. [[CrossRef](#)]
67. Mishra, V.N.; Rai, P.K.; Prasad, R.; Punia, M.; Nistor, M.M. Prediction of spatio-temporal land use/land cover dynamics in rapidly developing Varanasi district of Uttar Pradesh, India, using geospatial approach: A comparison of hybrid models. *Appl. Geomat.* **2018**, *10*, 257–276. [[CrossRef](#)]
68. Appiah, D.O.; Schröder, D.; Forkuo, E.K.; Bugri, J.T. Application of Geo-Information Techniques in Land Use and Land Cover Change Analysis in a Peri-Urban District of Ghana. *ISPRS Int. J. Geo-Inf.* **2015**, *4*, 1265–1289. [[CrossRef](#)]
69. Congraton, R.G.; Green, K. *Assessing the Accuracy of Remotely Sensed Data: Principles and Practices*, 2nd ed.; Taylor and Francis Group, LLC: Abingdon, UK, 2009.
70. Maingi, J.K.; Marsh, S.E. *An Accuracy Assessment of 1992 Landsat-MSS Derived Land Cover for the Upper San Pedro Watershed (U.S./Mexico)*; United States Environmental Protection Agency: Washington, DC, USA, 2002; p. 29.
71. Hua, A.K. Land Use Land Cover Changes in Detection of Water Quality: A Study Based on Remote Sensing and Multivariate Statistics. *J. Environ. Public Health* **2017**, *2017*, 1–12. [[CrossRef](#)]
72. Manonmani, R.; Suganya, G.M.D. Remote sensing and GIS application in change detection study in urban zone using multi temporal satellite. *Int. J. Geomat. Geo Sci.* **2010**, *24*, 60–65.
73. Liu, X.; Chen, B. Climatic warming in the Tibetan Plateau during recent decades. *Int. J. Climatol. A J. R. Meteorol. Soc.* **2000**, *20*, 1729–1742. [[CrossRef](#)]
74. Yan, L.; Liu, Z.; Chen, G.; Kutzbach, J.E.; Liu, X. Mechanisms of elevation-dependent warming over the Tibetan plateau in quadrupled CO<sub>2</sub> experiments. *Clim. Chang.* **2016**, *135*, 509–519. [[CrossRef](#)]
75. Harris, R. Rangeland degradation on the Qinghai-Tibetan plateau: A review of the evidence of its magnitude and causes. *J. Arid. Environ.* **2010**, *74*, 1–12. [[CrossRef](#)]
76. You, C.; Tjernström, M.; Devasthale, A. Eulerian and Lagrangian views of warm and moist air intrusions into summer Arctic. *Atmos. Res.* **2021**, *256*, 105586. [[CrossRef](#)]
77. Bibi, S.; Wang, L.; Li, X.; Zhou, J.; Chen, D.; Yao, T. Climatic and associated cryospheric, biospheric, and hydrological changes on the Tibetan Plateau: A review. *Int. J. Clim.* **2018**, *38*, e1–e17. [[CrossRef](#)]
78. Kang, S.; Zhang, Q.; Qian, Y.; Ji, Z.; Li, C.; Cong, Z.; Zhang, Y.; Guo, J.; Du, W.; Huang, J.; et al. Linking atmospheric pollution to cryospheric change in the Third Pole region: Current progress and future prospects. *Natl. Sci. Rev.* **2019**, *6*, 796–809. [[CrossRef](#)]
79. You, Q.; Wu, F.; Shen, L.; Pepin, N.; Jiang, Z.; Kang, S. Tibetan Plateau amplification of climate extremes under global warming of 1.5 °C, 2 °C and 3 °C. *Glob. Planet. Chang.* **2020**, *192*, 103261. [[CrossRef](#)]

80. Liu, Q.; Mayer, C.; Wang, X.; Nie, Y.; Wu, K.; Wei, J.; Liu, S. Interannual flow dynamics driven by frontal retreat of a lake-terminating glacier in the Chinese Central Himalaya. *Earth Planet. Sci. Lett.* **2020**, *546*, 116450. [[CrossRef](#)]
81. Yao, X.; Iqbal, J.; Li, L.-J.; Zhou, Z.-K. Characteristics of mountain glacier surge hazard: Learning from a surge event in NE Pamir, China. *J. Mt. Sci.* **2019**, *16*, 1515–1533. [[CrossRef](#)]
82. You, Q.; Wu, T.; Shen, L.; Pepin, N.; Zhang, L.; Jiang, Z.; Wu, Z.; Kang, S.; AghaKouchak, A. Review of snow cover variation over the Tibetan Plateau and its influence on the broad climate system. *Earth-Sci. Rev.* **2020**, *201*. [[CrossRef](#)]
83. Zemp, M.; Huss, M.; Thibert, E.; Eckert, N.; McNabb, R.W.; Huber, J.; Barandun, M.; Machguth, H.; Nussbaumer, S.U.; Gärtner-Roer, I.; et al. Global glacier mass changes and their contributions to sea-level rise from 1961 to 2016. *Nature* **2019**, *568*, 382–386. [[CrossRef](#)]
84. Fujita, K.; Kadota, T.; Rana, B.; Kayastha, R.B.; Ageta, Y. Shrinkage of Glacier AX010 in Shorong region, Nepal Himalayas in the 1990s. *Bull. Glaciol. Res.* **2001**, *18*, 51–54.
85. Orsolini, Y.; Wegmann, M.; Dutra, E.; Liu, B.; Balsamo, G.; Yang, K.; de Rosnay, P.; Zhu, C.; Wang, W.; Senan, R.; et al. Evaluation of snow depth and snow cover over the Tibetan Plateau in global reanalyses using in situ and satellite remote sensing observations. *Cryosphere* **2019**, *13*, 2221–2239. [[CrossRef](#)]
86. Shen, L.; Zhang, Y.; Ullah, S.; Pepin, N.; Ma, Q. Changes in snow depth under elevation-dependent warming over the Tibetan Plateau. *Atmos. Sci. Lett.* **2021**, *22*, e1041. [[CrossRef](#)]
87. Yang, M.; Wang, X.; Pang, G.; Wan, G.; Liu, Z. The Tibetan Plateau cryosphere: Observations and model simulations for current status and recent changes. *Earth-Sci. Rev.* **2018**, *190*, 353–369. [[CrossRef](#)]
88. Zheng, G.; Allen, S.K.; Bao, A.; Ballesteros-Cánovas, J.A.; Huss, M.; Zhang, G.; Li, J.; Yuan, Y.; Jiang, L.; Yu, T.; et al. Increasing risk of glacial lake outburst floods from future Third Pole deglaciation. *Nat. Clim. Chang.* **2021**, *11*, 411–417. [[CrossRef](#)]
89. Piao, S.; Cui, M.; Chen, A.; Wang, X.; Ciais, P.; Liu, J.; Tang, Y. Altitude and temperature dependence of change in the spring vegetation green-up date from 1982 to 2006 in the Qinghai-Xizang Plateau. *Agric. For. Meteorol.* **2011**, *151*, 1599–1608. [[CrossRef](#)]
90. Liu, Y.; Fan, J.; Harris, W.; Shao, Q.; Zhou, Y.; Wang, N.; Li, Y. Effects of plateau pika (*Ochotona curzoniae*) on net ecosystem carbon exchange of grassland in the Three Rivers Headwaters region, Qinghai-Tibet, China. *Plant Soil* **2012**, *366*, 491–504. [[CrossRef](#)]
91. Jingsheng, W.; Xianzhou, Z.; Baoxiong, C.; Peili, S.; Junlong, Z.; Zhenxi, S.; Jian, T.; Jianshuang, W. Causes and Restoration of Degraded Alpine Grassland in Northern Tibet. *J. Resour. Ecol.* **2013**, *4*, 43–49. [[CrossRef](#)]
92. Yu, C.; Zhang, Y.; Claus, H.; Zeng, R.; Zhang, X.; Wang, J. Ecological and Environmental Issues Faced by a Developing Tibet. *Environ. Sci. Technol.* **2012**, *46*, 1979–1980. [[CrossRef](#)]
93. Wang, Z.; Wu, J.; Niu, B.; He, Y.; Zu, J.; Li, M.; Zhang, X. Vegetation Expansion on the Tibetan Plateau and Its Relationship with Climate Change. *Remote Sens.* **2020**, *12*, 4150. [[CrossRef](#)]
94. Na, L.; Genxu, W.; Guangsheng, L.; Yun, L.; Xiangyang, S. The ecological implications of land use change in the Source Regions of the Yangtze and Yellow Rivers, China. *Reg. Environ. Chang.* **2013**, *13*, 1099–1108. [[CrossRef](#)]
95. Myers-Smith, I.H.; Forbes, B.C.; Wilmking, M.; Hallinger, M.; Lantz, T.; Blok, D.; Tape, K.D.; Macias-Fauria, M.; Sass-Klaassen, U.; Lévesque, E.; et al. Shrub expansion in tundra ecosystems: Dynamics, impacts and research priorities. *Environ. Res. Lett.* **2011**, *6*, 045509. [[CrossRef](#)]
96. Myers-Smith, I.H.; Kerby, J.T.; Phoenix, G.K.; Bjerke, J.W.; Epstein, H.E.; Assmann, J.J.; John, C.; Andreu-Hayles, L.; Angers-Blondin, S.; Beck, P.S.; et al. Complexity Revealed in the Greening of the Arctic. *Nat. Clim. Chang.* **2020**, *10*, 106–117. [[CrossRef](#)]
97. Harsch, M.A.; Hulme, P.E.; McGlone, M.S.; Duncan, R.P. Are Treelines Advancing? A Global Meta-Analysis of Treeline Response to Climate Warming. *Ecol. Lett.* **2009**, *12*, 1040–1049. [[CrossRef](#)]
98. Wang, Z.; Luo, T.; Li, R.; Tang, Y.; Du, M. Causes for the unimodal pattern of biomass and productivity in alpine grasslands along a large altitudinal gradient in semi-arid regions. *J. Veg. Sci.* **2012**, *24*, 189–201. [[CrossRef](#)]
99. Chen, B.; Zhang, X.; Tao, J.; Wu, J.; Wang, J.; Shi, P.; Zhang, Y.-J.; Yu, C. The impact of climate change and anthropogenic activities on alpine grassland over the Qinghai-Tibet Plateau. *Agric. For. Meteorol.* **2014**, *189–190*, 11–18. [[CrossRef](#)]
100. Tian, Y.; Liu, B.; Hu, Y.; Xu, Q.; Qu, M.; Xu, D. Spatio-Temporal Land-Use Changes and the Response in Landscape Pattern to Hemeroby in a Resource-Based City. *ISPRS Int. J. Geo-Inf.* **2020**, *9*, 20. [[CrossRef](#)]
101. Sun, Z.B.; Gao, M.H.; Cui, X.F. Land use change in north slope economic zone of Tianshan Mountain based on remote sensing and GIS from 2000–2015. *J. Beijing Norm. Univ. Nat. Sci.* **2018**, *54*, 397–404.
102. Che, M.; Chen, B.; Innes, J.L.; Wang, G.; Dou, X.; Zhou, T.; Zhang, H.; Yan, J.; Xu, G.; Zhao, H. Spatial and Temporal Variations in the End Date of the Vegetation Growing Season Throughout the Qinghai–Tibetan Plateau from 1982 to 2011. *Agric. For. Meteorol.* **2014**, *189*, 81–90. [[CrossRef](#)]
103. Luo, Z.; Wu, W.; Yu, X.; Song, Q.; Yang, J.; Wu, J.; Zhang, H. Variation of Net Primary Production and Its Correlation with Climate Change and Anthropogenic Activities over the Tibetan Plateau. *Remote Sens.* **2018**, *10*, 1352. [[CrossRef](#)]
104. Zhu, L.; Meng, J.; Li, F.; You, N. Predicting the patterns of change in spring onset and false springs in China during the twenty-first century. *Int. J. Biometeorol.* **2017**, *63*, 591–606. [[CrossRef](#)] [[PubMed](#)]
105. Nepal, S.; Khatiwada, K.R.; Pradhananga, S.; Kralisch, S.; Samyn, D.; Bromand, M.T.; Jamal, N.; Dildar, M.; Durrani, F.; Rassouly, F.; et al. Future snow projections in a small basin of the Western Himalaya. *Sci. Total. Environ.* **2021**, *795*, 148587. [[CrossRef](#)]
106. Duan, K.; Yao, T.; Wang, N.; Liu, H. Numerical simulation of Urumqi Glacier No. 1 in the eastern Tianshan, central Asia from 2005 to 2070. *Chin. Sci. Bull.* **2012**, *57*, 4505–4509. [[CrossRef](#)]

107. Li, Y.; Tian, L.; Yi, Y.; Moore, J.C.; Sun, S.; Zhao, L. Simulating the Evolution of Qiangtang No. 1 Glacier in the Central Tibetan Plateau to 2050. *Arct. Antarct. Alp. Res.* **2017**, *49*, 1–12. [[CrossRef](#)]
108. Adhikari, S.; Huybrechts, P. Numerical Modelling of Historical Front Variations and the 21st-Century Evolution of Glacier AX010, Nepal Himalaya. *Ann. Glaciol.* **2009**, *50*, 27–34. [[CrossRef](#)]
109. Kathayat, G.; Cheng, H.; Sinha, A.; Yi, L.; Li, X.; Zhang, H.; Li, H.; Ning, Y.; Edwards, R.L. The Indian monsoon variability and civilization changes in the Indian subcontinent. *Sci. Adv.* **2017**, *3*, e1701296. [[CrossRef](#)] [[PubMed](#)]
110. Linsbauer, A.; Frey, H.; Haeberli, W.; Machguth, H.; Azam, M.; Allen, S. Modelling glacier-bed overdeepenings and possible future lakes for the glaciers in the Himalaya—Karakoram region. *Ann. Glaciol.* **2016**, *57*, 119–130. [[CrossRef](#)]
111. Yang, K.; Lu, H.; Yue, S.; Zhang, G.; Lei, Y.; La, Z.; Wang, W. Quantifying Recent Precipitation Change and Predicting Lake Expansion in the Inner Tibetan Plateau. *Clim. Chang.* **2018**, *147*, 149–163. [[CrossRef](#)]